10-30-2009

Fold and thrust partitioning in a contracting fold belt: Insights from the 1931 Mach earthquake in Baluchistan

Walter Szeliga
Central Washington University, walter@geology.cwu.edu

Roger Bilham
University of Colorado at Boulder

Daniel Schelling
Structural Geology International, LLC,

Din Mohamed Kakar
University of Baluchistan,

Sarosh Lodi
NED University

Recommended Citation
Szeliga, W., et al. (2009). Fold and thrust partitioning in a contracting fold belt: Insights from the 1931 Mach earthquake in Baluchistan. *Tectonics, 28*, TC5019. DOI: 10.1029/2008TC002265

Fold and thrust partitioning in a contracting fold belt: Insights from the 1931 Mach earthquake in Baluchistan

Walter Szeliga,[1] Roger Bilham,[1] Daniel Schelling,[2] Din Mohamed Kakar,[3] and Sarosh Lodi[4]

Received 21 January 2008; revised 27 October 2008; accepted 8 July 2009; published 30 October 2009.

[1] Surface deformation associated with the 27 August 1931 earthquake near Mach in Baluchistan is quantified from spirit-leveling data and from detailed structural sections of the region interpreted from seismic reflection data constrained by numerous well logs. Mean slip on the west dipping Dezghat/Bannh fault system amounted to 1.2 m on a 42 km × 72 km thrust plane with slip locally attaining 3.2 m up dip of an inferred locking line at ~9 km depth. Slip also occurred at depths below the interseismic locking line. In contrast, negligible slip occurred in the 4 km near the interseismic locking line. The absence of slip here in the 4 years following the earthquake suggests that elastic energy there must either dissipate slowly in the interseismic cycle, or that a slip deficit remains, pending its release in a large future earthquake. Elastic models of the earthquake cycle in this fold and thrust belt suggest that slip on the frontal thrust fault is reduced by a factor of 2 to 8 compared to that anticipated from convergence of the hinterland, a partitioning process that is presumably responsible for thickening of the fold and thrust belt at the expense of slip on the frontal thrust. Near the latitude of Quetta, GPS measurements indicate that convergence is ~5 mm/yr. Hence the minimum renewal time between earthquakes with 1.2-m mean displacement should be as little as 240 years. However, when the partitioning of fold belt convergence to frontal thrust slip is taken into account the minimum renewal time may exceed 2000 years. **Citation:** Szeliga, W., R. Bilham, D. Schelling, D. M. Kakar, and S. Lodi (2009), Fold and thrust partitioning in a contracting fold belt: Insights from the 1931 Mach earthquake in Baluchistan, *Tectonics*, *28*, TC5019, doi:10.1029/2008TC002265.

1. Introduction

[2] Between 1931 and 1935 three major earthquakes occurred between the Bolan Pass and Quetta in the Baluchistan province of Pakistan. The first of these, an Mw 6.8 event near Sharigh (2135 UT, 24 August 1931), was followed 66 h later by the Mach Mw 7.3 earthquake (1527 UT, 27 August). The third and largest earthquake was the Mw 7.7 30 May 1935 earthquake that destroyed 90% of Quetta and caused 35,000 deaths [*Ambraseys and Bilham*, 2003]. Because no similar magnitude earthquakes occurred in the 3 decades before or after this sequence, it is very probable that static or dynamic triggering of these nearby earthquakes is responsible for their clustering in time.

[3] All three earthquakes lie within the 150-km-wide zone of deformation between the Asian and Indian plates, a region bounded to the west by the Chaman fault and to the east by the Indus plain [*Bender and Raza*, 1995] (Figure 1a). The strike-slip component of slip on the plate boundary is estimated to be 33 cm/yr from global GPS closure estimates [*Apel et al.*, 2006] and 31 mm/yr from paleomagnetic reconstructions of the Indian Ocean seafloor [*Molnar and Stock*, 2009]. Geological estimates of slip on the Chaman fault system [*Lawrence et al.*, 1992] indicate slip rates of 19–24 mm/yr in the past 20 Myr and 25–35 mm/yr for the past 2 Myr [*Beun et al.*, 1979; *Lawrence et al.*, 1992], suggesting that as much as one third of this shear signal may be distributed in the fold belt. The plate boundary is regionally transpressive and from seismic moment release calculations in the past 200 years, and from the inferred obliquity of the plate boundary to the local slip vector between India and Asia it has been estimated that strain partitioning results in convergence of the fold belts of up to 13 ± 3 mm/yr [*Ambraseys and Bilham*, 2003]. This estimate is probably inflated by the seismic productivity of the past century, which may be abnormally high if the earthquakes presently under discussion are atypical of long-term seismicity. A lower convergence rate is obtained from analog and numerical modeling of the strain in the region (3–6 mm/yr NW/SE shortening [*Bernard et al.*, 2000; *Haq and Davis*, 1997]), and this lower rate is consistent with preliminary GPS measurements north of Quetta presented in this paper.

[4] Although triangulation data exist in the region no remeasurements have been published [*Ambraseys and Bilham*, 2003]. However, a first-order spirit leveling line, first measured in 1909 between Sukkur and Chaman, was remeasured shortly after the 1935 Quetta earthquake [*Wilson*, 1938]. Parts of the line were raised 65 cm where they crossed the frontal thrusts of the northern Kirthar Range to the west of Sibi, exceeding the combined errors in the survey by more than an order of magnitude. A preliminary analysis of these data (Figure 2a) in the absence of geological constraints, concluded that the asymmetry in the vertical deformation, if caused by planar slip, was caused by 1–1.2 m of slip on an east dipping blind thrust fault between 1 km depth and

[1] CIRES and Department of Geological Sciences, University of Colorado, Boulder, Colorado, USA.
[2] Structural Geology International, LLC, Salt Lake City, Utah, USA.
[3] Department of Geology, University of Baluchistan, Quetta, Pakistan.
[4] Department of Civil Engineering, NED University, Karachi, Pakistan.

0278-7407/09/2008TC002265

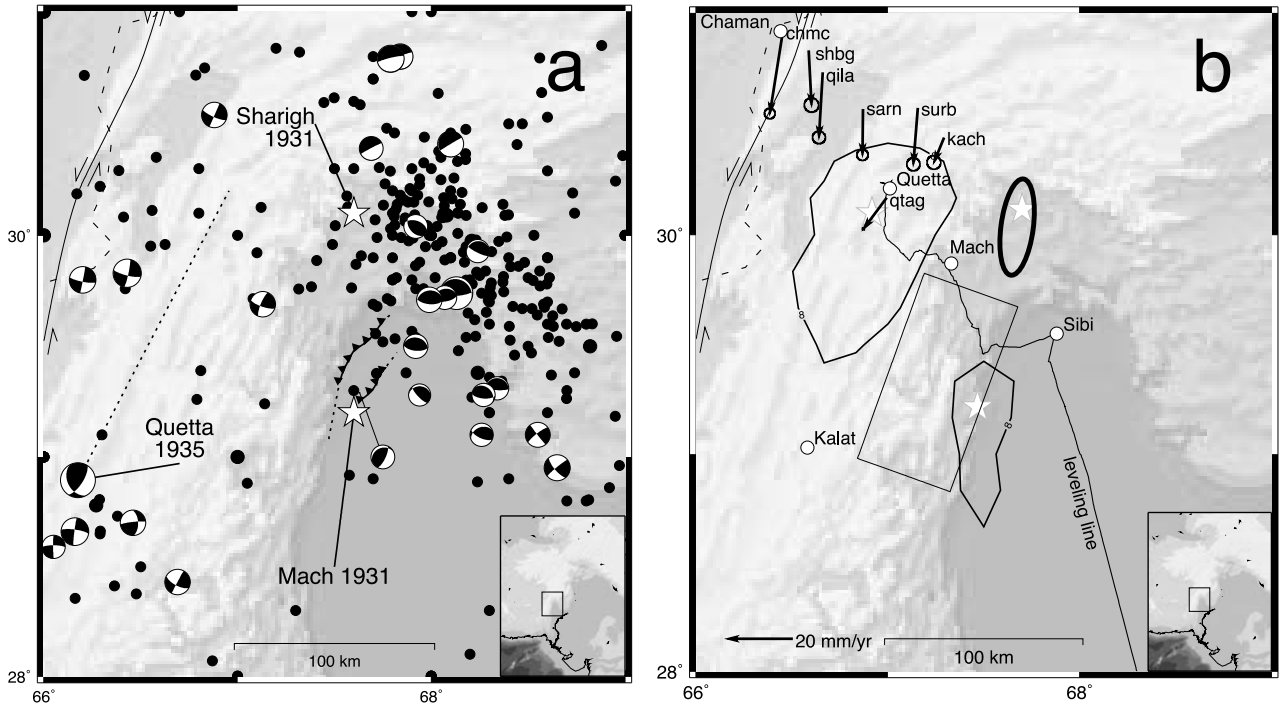

Figure 1. (a) Recent seismicity (Mw > 5) and instrumental locations for the Sharigh, Mach (stars), and Quetta earthquakes (focal mechanism beach ball) and their inferred causal faults (Quetta rupture dashed and Bannh fault shown as surface thrust NE of the instrumental epicenter). Focal mechanisms are scaled according to magnitude: the largest focal mechanism is Mw 7.7 [from *Singh and Gupta*, 1980] and the smallest is Mw = 5 (all from the Harvard MCT). (b) Interpolated intensity VIII isoseismals for the three earthquakes, the path of the 1909–1936 leveling line, and GPS velocity vectors 2005–2008 relative to fixed India. The approximate rupture zone of the Mach earthquake is shown by the rectangle. The intensity-derived epicenters are shown on each map as a star. The Quetta centroid solution lies at the opposite end of the rupture from the intensity solution as a result of directivity.

~25 km depth [*Ambraseys and Bilham*, 2003]. The fit between observed surface deformation and synthetic planar slip was appealing, but the asymmetry of the uplift signal required a counterintuitive easterly dip to the frontal thrust. The description of a wedge-thrust geometry with an east dipping shallow ramp at this location in the literature, however, appeared to confirm its presence [*Banks and Warburton*, 1986]. Yet, when the surface deformation associated with slip on the two faults of their triangle zone was examined in detail by *Garcia et al.* [2006], no combination of slip was found that

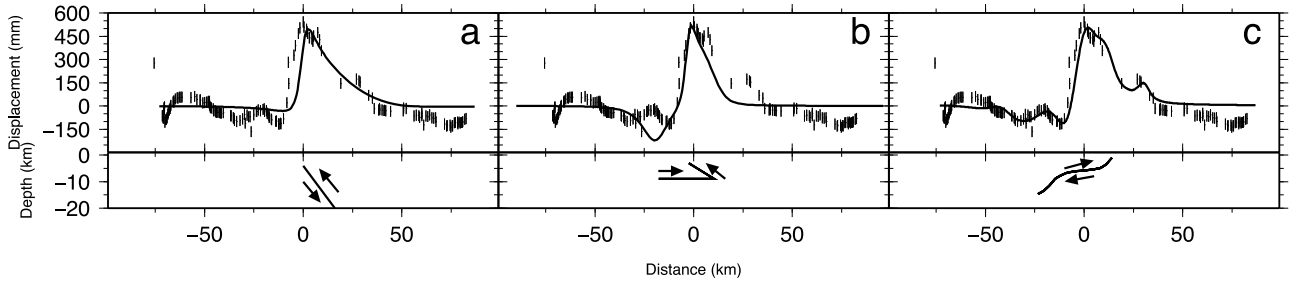

Figure 2. Schematic sections of vertical deformation and subsurface geometry of previous attempts to emulate observed uplift data in the Mach earthquake (Figures 2a and 2b). These models invoked uniform subsurface slip on shallow east dipping planar thrusts. (a) Planar, uniform slip is invoked with no structural control [*Ambraseys and Bilham*, 2003]. (b) The speculative wedge thrust geometry of *Banks and Warburton* [1986] constrains two fault planes on which combinations of uniform slip were imposed to obtain the best fitting surface uplift [*Garcia et al.*, 2006]. (c) Spatially variable slip on the west dipping Bannh fault [*Bannert et al.*, 1992; *Schelling*, 1999] is investigated in this paper.

resulted in an improved fit to the leveling data (Figure 2b). Models with more complex geometries also failed to improve the fit.

[5] The two previous interpretations, based as they were on limited structural information may now be discarded due to the availability of seismic reflection data from the Sibi and Mach areas, controlled by stratigraphic information from numerous boreholes. We present structural interpretations in section 2 that demonstrate that the frontal thrusts of the Kirthar range west of Sibi dip to the west [*Bannert et al.*, 1992; *Schelling*, 1999].

2. Structural Setting of the Bolan Pass Region

[6] The Bolan Pass region of Baluchistan (Figure 3) is located along the deformation front of the northern Kirthar Range, where north-south trending structural systems (folds and thrust faults) of the Kirthar Range give way to the more complexly oriented structural systems of the Quetta Syntaxis. Detailed structural field work carried out in the Bolan Pass region and elsewhere in the Kirthar Range during the late 1990s [*Schelling*, 1999] indicates that the deformation front of the northern Kirthar Range is dominated by east vergent, contractional fold-fault systems that give way to strike-slip oriented fault systems along and to the west of the Quetta Plateau. In addition, surface structural data has allowed the geometries and orientations of fold-fault pairs to be defined across and along the mountain front at different tectonostratigraphic levels in the Bolan Pass region. Surface structural geometries from the Bolan Pass have been projected to depth, and in conjunction with interpreted seismic data from the Bolan Pass and adjacent Sibi Trough areas, a balanced structural cross section has been constructed across the Bolan Pass in the vicinity of the leveling line examined in this paper (Figure 4).

[7] As shown on the cross section of Figure 4, the frontal structural system of the Bolan Pass area is defined by an east vergent, asymmetric fault propagation fold (the Dezghat Anticline) and underlying, west dipping thrust fault system that is known from seismic data to flatten near the base of the Siwalik Group, a roughly 6-km-thick stratigraphic section of Miocene-Pliocene sandstone, shale, and conglomerate that define foreland basin fill to the actively subsiding Sibi Trough (Indus Basin). Tectonic shortening across the Dezghat Anticline and associated thrust faults is on the order of several kilometers (Figure 4). However, all of the structural uplifts identified to the west of the Dezghat Anticline are known from surface and subsurface structural data to involve the Jurassic Chiltan Limestone and overlying Cretaceous through Eocene stratigraphic section, including the Goru and Sembar formations, the Parh and Dunghan limestones, the Ghazij Shale, and the Kirthar Limestone (Figure 4). Between the Parhi Jhal Anticline mapped to the west of the Bolan Pass and the Sibi Trough located to the east of the Kirthar Range, structural uplift of the Chiltan Limestone is on the order of 9 to 10 km (Figure 4), and associated tectonic shortening across the same structural systems, as determined from surface and subsurface data, is estimated at $\sim$15 km. This requires that thrust faults exposed at the surface and that involve the Chiltan Limestone are relatively high angle structural features, with measured, near-surface dips of roughly 60° and estimated fault angles of 30° to 45° at 10 to 20 km depth (Figure 4). In addition, 9 to 10 km of uplift across the combined Bolan Pass and Parhi Jhal Anticlines requires a mid-crustal décollement surface at a depth of 18 to 20 km beneath the Quetta Plateau, as indicated on the cross section of Figure 4. This 18- to-20-km décollement depth is well below the projected, base-Triassic stratigraphic level of known lithology from the Kirthar and nearby Sulaiman mountain ranges, and therefore, the lithology at the basal décollement level beneath the Quetta Plateau remains unknown and may actually be located in basement rocks.

[8] Additional décollement surfaces of the Kirthar Range have been identified within the Eocene Ghazij Shale, which separates the underlying, competent carbonates of the Chiltan-Dunghan limestones from the overlying Kirthar Limestone and Siwalik Group (Figure 4). Significant deformation associated with these Ghazij Shale décollement surfaces is restricted to an area above the subsurface, frontal fault ramp identified beneath the Bolan Pass, where the underlying (basal) décollement surface to the Kirthar Range climbs from a depth of 18 km or more beneath the Parhi Jhal and Bolan Pass Anticlines to the upper, basal Siwalik Group décollement surface identified beneath the Dezghat Anticline at roughly 6 km depth. Thrust faults originating within the Ghazij Shale result in short (several hundred meters) wavelength anticline-syncline pairs and the development of exposed back thrust surfaces along the east limb of the Bolan River Anticline. These latter fold-fault systems have accommodated less than 1 km of tectonic shortening, though as exposed structural systems in the Bolan Pass area there is little question that thrust faults originating within the Ghazij Shale will affect surface deformation across the Bolan Pass area, as indicated from the leveling data discussed in this paper.

3. GPS Measurements of Convergence and Shear Between the Asian and Indian Plates

[9] GPS measurements in Pakistan are historically of limited coverage and duration. Campaign measurements from six sites with locations between the town of Chaman, 30 km west of the Chaman fault, and the town of Kach, $\sim$70 km NE of Quetta, have been measured at least twice in the period 2006–2008 and compared to continuous measurements made in Karachi (not shown) and Quetta (qtag) (Figure 1b). The continuous points in Pakistan are operated from flat-roofed concrete frame buildings and the campaign points are measured on bipods set on stainless steel screws cemented into exposed rock. GPS observations were recorded either with Trimble NetRS, 5700 or R7 receivers using a 30 s sampling rate, and processed using an elevation cutoff angle of 10°. Campaign data have durations of 3–7 days from each site. The daily data from these sites were processed along with data from 10 regional IGS stations using GAMIT version 10.34 [*King and Bock*, 2002]. The regional solutions were then combined with global solutions from SOPAC (ftp://garner.ucsd.edu/pub/hfiles) using GLOBK/GLORG

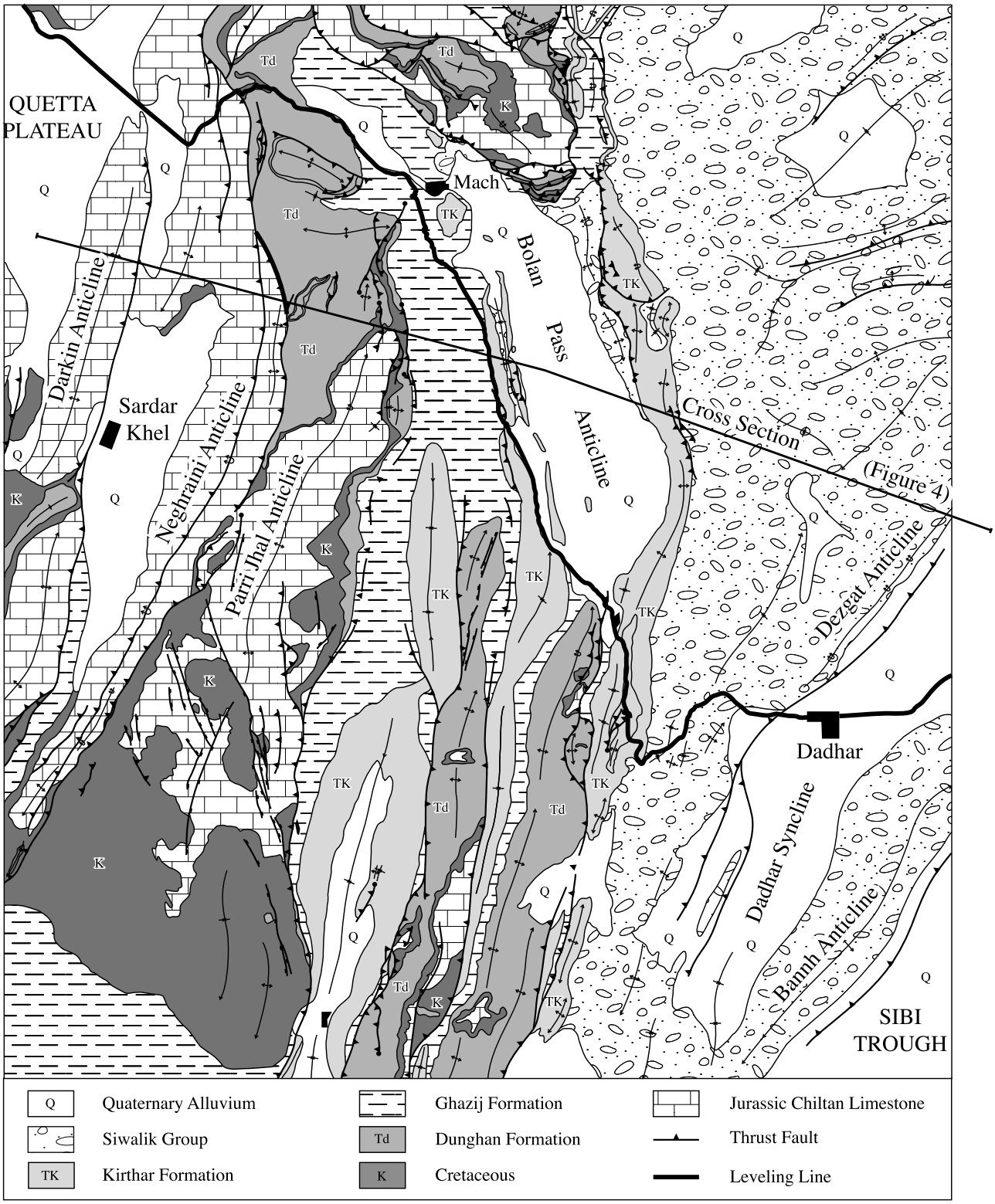

Figure 3. Geological map of the Bolan Pass region of the northern Kirthar Range, showing the locations of the balanced structural cross section and leveling line discussed in the paper.

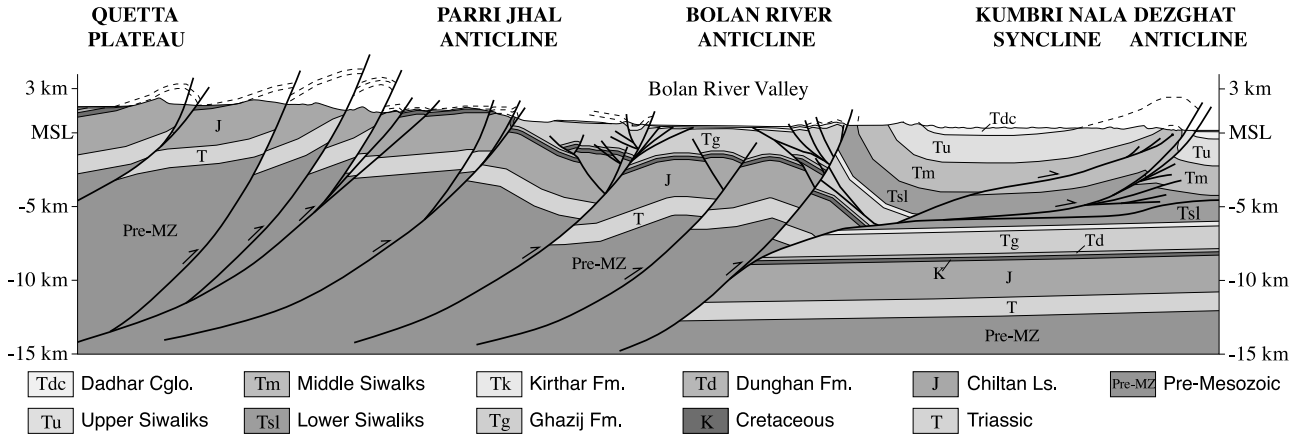

Figure 4. Balanced structural cross section across the deformation front of the northern Kirthar Range in the Bolan Pass area and in the vicinity of the leveling line. See Figure 3 for cross section location and text for discussion.

version 5.16 [*Herring*, 2002] to determine time series and velocities in the ITRF2005 reference frame. These velocities were then transformed into an Indian plate-fixed reference frame using pole of rotation parameters determined by *Bettinelli et al.* [2006].

[10] The processed campaign GPS data are associated with formal uncertainties of ±3 mm/yr, and the continuous data are associated with uncertainties of ±1 mm/yr (Figure 5). Not shown Figure 5 are the velocity vectors for Karachi and Nagar Parkar (north of the 2001 Bhuj earthquake) that move at approximately the velocity of the Indian plate suggesting that little deformation occurs across the Indus delta, or near the Bhuj region. The SSW velocity of Quetta is anomalous relative to the points on the east-west transect through Chaman. It is possible that the proximity of the city to the fault that slipped in 1935 may influence the azimuth of its vector, and we have accordingly established additional points to the southeast of Quetta to search for local deformation; however, these data are currently too noisy to be of value to the present study. InSAR imagery shows no evidence for a region of subsidence near Quetta caused by groundwater withdrawal (S. P. Satyabala, personal communication, 2008). The most easterly point on the traverse, Kach, is also anomalous in that it shows no convergence with India. We note that Kach lies close to the Harnai fault at the confluence of north striking and west striking structures and its velocity vector may thus be influenced by local tectonics.

[11] Thus, our limited view of motions within this complex region of shear and convergence afforded by the GPS data permit only the simplest of interpretations at present. In Figure 5 we show the form of the velocity field anticipated from simple shear at depth. The curve shown is that corresponding to 31 mm/yr of left lateral slip on the Chaman fault below 12 km depth, a locking depth consistent with the depths of seismicity observed near the Chaman fault [*Ambraseys and Bilham*, 2003], but the uncertainties in the data permit both shallower or deeper locking depths and a much reduced slip velocity. That four of the campaign data points are systematically misfit by this simple view of shear

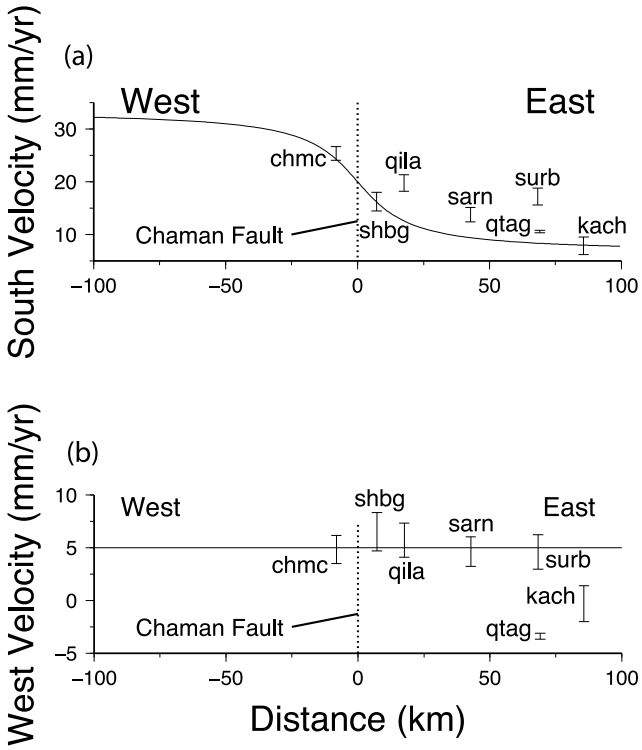

Figure 5. (a) GPS velocities projected east-west showing southward velocities relative to stable India. For locations, see Figure 1b. The curve indicates the elastic velocity field calculated for a shear dislocation on the Chaman fault slipping at 31 mm/yr below a locked depth of 12 km. (b) GPS velocities projected east-west showing westward velocities relative to stable India. For locations, see Figure 1b. The GPS points, with two exceptions, show convergence with fixed India at 5 ± 1 mm/yr. The two exceptions (see text) are at Kach and Qtag (the continuous GPS point at Quetta).

Table 1. Instrumental and Inferred Macroseismic Locations for the Three Earthquakes

Event	Date	Instrumental Epicenter	Mw	Minimum Magnitude Epicenter	Mi	Minimum Variance Epicenter
Sharigh	24 Aug 1931	31.1°N, 67.7°E	6.8	29.87°N, 67.62°E	5.9	30.12°N, 67.60°E
Mach	27 Aug 1931	29.9°N, 67.6°E	7.3	29.55°N, 67.55°E	7.2	29.22°N, 67.47°E
Quetta	30 May 1935	28.87°N, 66.4°E	7.7	30.10°N, 66.92°E	7.6	30.18°N, 66.92°E

suggests that the surface structures are moving relative to the basement as anticipated by structural models of thin skinned tectonics in the region [*Bernard et al.*, 2000; *Haq and Davis*, 1997].

[12] We interpret the mean westward translation of five of the seven GPS points depicted in Figures 1b and 5 toward the Indian plate at 5 ± 1 mm/yr as indicative of the transpressional convergence of the Sulaiman fold belt, which we use as a proxy for maximum convergence rates in the Kirthar range. The GPS measurements were obtained north of Quetta at ~30°N, where the fold belt is significantly wider than at the latitude of the Mach earthquake. The lower transpressional obliquity of the Chaman system south of 30°N, and its narrower width, suggests that convergence occurs there at a lower rate. We cannot as yet quantify this from direct observation but we assume that the rate is at least half that of the rate measured north of Quetta, i.e., current east-west convergence near the epicenters of the Quetta and Mach earthquakes is probably 2.5 to 5 mm/yr.

4. Macroseismic Location of the Mach Earthquake

[13] The Mach earthquake is named for the railway headquarters at Mach that were heavily damaged in the earthquake [*Ambraseys and Bilham*, 2003]. The jail was destroyed, and 400 prisoners were briefly at large. Although no surface rupture was recorded, the parapets of a 140-m-long approximately E-W bridge converged 20 cm without being tilted. Numerous rockfalls occurred at the time of the earthquake raising clouds of dust near Mach and the Bolan Pass to the SE.

[14] Although instrumental locations and magnitudes are available for the 1931 and 1935 earthquakes (Figure 1 and Table 1), additional knowledge of the extent and azimuth of their rupture zones can be inferred from intensity data recorded for each event. The data are available in the form of damage reports to structures near their epicenters, and from felt reports at larger distances. Previous analysis of the intensity data for the Sharigh, Mach and Quetta earthquakes have interpolated isoseismal contours for a range of intensities to determine the most probable location of their rupture zones. Banana-shaped isoseismals drawn by *West* [1934] for the highest intensities are distorted by the uneven coverage of his data. *Ambraseys and Bilham* [2003] reevaluated these data supplemented by additional observations and concluded that the highest isoseismals for the second two earthquakes form north elongated polygons (Figure 1b). Insufficient data for the Sharigh earthquake were available to form definitive conclusions, except that its epicentral location was close to the town of that name.

[15] We have subjected these same observed intensities to a more rigorous analysis using the methods of *Bakun and Wentworth* [1997]. This approach does not contour isoseismals but instead contours the most probable locations for the epicenter using a grid search and assumptions about attenuation of shaking intensity with distance. The method uses recent earthquakes from elsewhere in the region for which location and magnitude are known and for which intensity data are also available, to quantify the attenuation of shaking intensity with distance [*Szeliga et al.*, 2009]. The method then calculates the most likely magnitude for the earthquake, were it to have occurred at points on a hypothetical regularly spaced grid centered on the centroid of maximum intensities. The resulting values on the grid are then contoured to provide a series of isomagnitude contours surrounding a closed contour of minimum magnitude for the earthquake. The center of this minimum contour is the epicentral location of the smallest possible earthquake that could have caused the observed intensity distribution (Figure 6 and Table 1). If observations are noise free, well distributed in intensity range, and endowed with good azimuthal coverage, these contours tend to be elliptical or circular; however, if the coverage is azimuthally poor, or of low quality, the resulting contours may be complex with multiple minima.

[16] The magnitude contours provide no estimate of the variance between magnitudes predicted from each observation at each point in the grid search. A new set of contours is generated based on the variance of the magnitude estimates derived for each point on the grid were the earthquake to have occurred at that point. When these variances are contoured, a region of minimum variance is obtained, usually, but not always, close to the minimum magnitude solution. For the three earthquakes in Baluchistan the minimum magnitude locations are indeed close to their minimum variance locations, typical of an acceptable macroseismic solution (Table 1). The minimum variance contours are assigned probabilities, with the most probable location for the epicenter being the location of minimum variance. The intersection of the minimum variance location with a contour of the isomagnitude solution indicates the most probable magnitude for the earthquake.

[17] The solutions for all three earthquakes are listed in Table 1 and are shown in Figure 6. The absence of complexity to the minimum magnitude contours and their coincidence with the marginally more complex minimum variance locations in each case is notable. The most probable location for the Mach epicenter lies near the southern end of its rupture zone and near its instrumental location. We ignore the smaller minimum noted north of Sibi. In contrast the location of the minimum variance epicenter for the 1935 Quetta earthquake lies near Quetta, more than 130 km NNE of the instrumental

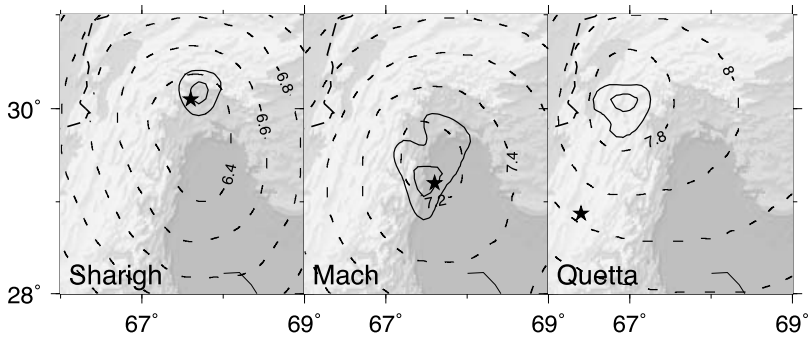

Figure 6. Macroseismc epicenters for the Sharigh, Mach, and Quetta earthquakes. The dashed contours are not isoseismals but isomagnitude contours using the method of *Bakun and Wentworth* [1997]. They indicate the required magnitude for each earthquake had it been located on these contours. The preferred macroseismic epicentral location lies within the closed contour of the minimum-variance solution shown as solid lines, while the stars represent the instrumentally located epicenters.

location for the earthquake. We assume that the high intensities reported from Quetta were enhanced by directivity in the direction of rupture propagation [*Singh and Gupta*, 1980; *Day et al.*, 2008]. The minimum variance epicentral location for the Sharigh event is found to be approximately to the north of the Mach event, west of the epicentral location inferred by earlier investigations; however, similar to previous investigations of this earthquake, we are unable to identify a specific causal fault.

[18] Using the constants derived by *Bakun and Wentworth* [1997] for California, we infer the Mach magnitude to have been Mw 7.2 in good agreement with the value of Mw 7.3 derived by *Ambraseys and Bilham* [2003], but the inferred magnitude for the Sharigh event is significantly smaller, Mw 5.9 instead of 6.8, probably the result of the sparse sampling of macroseismic data points for this event. Use of constants derived by *Szeliga et al.* [2009] yield similar epicentral locations but with lower magnitudes for all three earthquakes. Our preferred location for the Sharigh event lies to the west of previously inferred locations, but no causal fault can be identified there from geological evidence or microseismicity. Recent CMT solutions [*Giardini et al.*, 1985; *Dziewonski et al.*, 1999] in the area (Figure 1a) indicate that the newly located Sharigh event lies in a transition region between NW-SE directed compression in the Bolan Pass region and N-S compression to the north. Focal mechanisms nearest to the epicenter of the Sharigh earthquake show a combination of NE dipping thrust faulting and thrusting along N-S directed décollements.

5. Leveling Data

[19] The Sukkur-Quetta leveling line (Figures 1b and 7) was originally surveyed between 1909 and 1914 with a benchmark spacing of 2–5 km [*Wilson*, 1938; *Ambraseys and Bilham*, 2003]. The leveling data are associated with random errors that grow with the square root of the distance traversed (L km) as $k\sqrt{L}$ mm, where k = 0.65, a constant

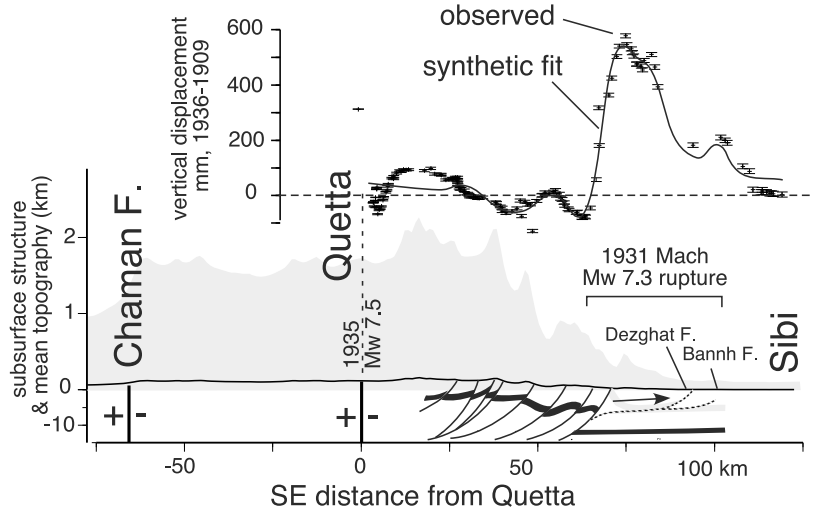

Figure 7. Leveling data, topographic relief, and subsurface section simplified from Figure 4. The synthetic fit to the data results from spatially varying slip on the Dezghat and Bannh faults (dashed line on section).

Table 2. Observed and Synthetic Slip on the Décollement[a]

Distance (km)	Depth (km)	Length (km)	Dip	Obs (m)	No Lock (m)	Co-8 (m)	Co-9 (m)	Interseismic (m)
104	−3.5	3.03	7.9	0.28	0.86	0.47	0.463	0
101	−3.92	3.01	5.14	0.35	1.34	0.72	0.713	0
98	−4.19	3.01	3.39	0.3	1.71	0.9	0.901	0
95	−4.36	3	2.51	0.36	2.03	1.06	1.06	0
92	−4.5	3	2.47	0.35	2.32	1.21	1.21	0
89	−4.62	3	3.28	0.4	2.62	1.34	1.35	0
86	−4.8	3.01	4.96	0.76	2.91	1.48	1.5	0
83	−5.06	3.03	7.63	1.17	3.2	1.61	1.63	0
80	−5.46	3.01	4.33	1.21	3.42	1.69	1.73	0
77	−5.69	3.01	3.83	1.63	3.6	1.73	1.79	0
74	−5.89	3.01	3.68	2.49	3.75	1.73	1.83	0
71	−6.08	3.03	7.77	3.16	3.93	1.7	1.84	0
68	−6.49	3.03	12.79	2.86	4.2	1.59	1.81	0
65.05	−7.16	3.02	28.75	1.56	4.64	1.31	1.71	0
62.4	−8.61	3	29.88	0.68	4.96	0	1.37	0
59.8	−10.11	3.02	12.13	0.54	5.29	0	0	1.6
56.85	−10.74	3.01	5.68	0.84	5.68	0	0	2.45
53.85	−11.04	3.01	4.22	1.04	6.04	0	0	3.16
50.85	−11.26	3.01	3.63	0.9	6.35	0	0	3.8
47.85	−11.45	3	2.38	0.68	6.65	0	0	4.39
44.85	−11.58	3	1.96	0.65	6.95	0	0	4.97
41.85	−11.68	3	1.71	0.66	7.27	0	0	5.56
38.85	−11.77	3	1.49	0.42	7.61	0	0	6.16
35.85	−11.85	3	1.29	0.09	7.99	0	0	6.81
32.85	−11.91	3	1.11	0.33	8.43	0	0	7.53
29.85	−11.97	3	0.96	0.96	8.98	0	0	8.41
26.85	−12.02	400.02	0.57	0.48	10	0	0	10

[a]Segments are free to slip in response to 10 m of thrust displacement imposed on the deepest fault segment, a value scaled to approximate the mean observed coseismic slip. Co-8 refers to coseismic slip shallower than ~8 km depth, and Co-9 refers to coseismic slip from one segment deeper, at ~9 km depth. "No Lock" indicates the slip that would occur in the absence of interseismic locking, and Interseismic indicates the synthetic slip that occurs below a locking line at 9 km depth. We have scaled the driving element to 10 km so that that synthetic slip approximates the mean slip derived from the observed leveling data.

derived from circuit closure errors in India [*Lenox-Conyngham*, 1916]. In addition, a systematic height-dependent error is present in the data that is typically less than 1×10^{-6} of the height above the starting point of the line in kilometers. The 65 cm of vertical deformation near the Bolan Pass exceeds systematic and random errors in the data by more than an order of magnitude. The leveling bench marks were georeferenced from $1'' = 1$ mile topographic sheets and have resulting uncertainties of up to 30 m (listed by *Ambraseys and Bilham* [2003]). We project these irregularly spaced leveling data at N110°E along a line perpendicular to the trend of folding in the Kirthar range (Figure 7).

[20] No surface rupture was reported for the 1931 Mach earthquake, although it is possible that *West*'s [1934] postseismic investigations did not include traverses across the frontal thrusts of the Kirthar range except near Sibi. To proceed with the analysis of the leveling data, we assume that slip on one or more of the mapped subsurface faults was responsible for the observed uplift. We digitized these subsurface faults from the geological cross sections, forming curved fault segments from a series of contiguous, 3-km-wide, planar segments. We then permitted various combinations of contiguous segments to slip. Each segment with nonzero slip contributes to the surface deformation field [*Okada*, 1992], and we searched for smooth distributions of slip on contiguous segments that most precisely produced the observed surface deformation. The analytical procedure that we adopted was to shift the surface projection of the parameterized faults relative to the leveling data and to invert for slip using the Green's functions for each segment. By minimizing the sum of squared residuals, we determined the optimal offset between the leveling data and our modeled geometry.

[21] The misfit between the parameterized faults and the projected leveling data is minimized with slip on deep segments of the Dezgat Thrust with contiguous slip on segments of the Bannh fault which branches from it eastward toward the surface (Figure 7). Maximum observed slip of 3.2 m occurs in segments between 7 and 5 km depth, updip from an inferred interseismic locking line at 8 or 9 km depth, where we observe minimum slip. The location of inferred interseismic locking is not constrained by observations of interseismic deformation, and hence there exists some uncertainty as to its true location; however, in section 6 we undertake additional numerical models that are consistent with this identification. A deeper locking line would decrease the inferred along strike length of the Mach rupture. The total width of the rupture above our 9-km-deep locking line is 42 km and the mean slip is 1.2 m (Table 2). Assuming a seismic moment of 1.1×10^{27} dyn cm, and that all the slip occurred seismically, the best fit slip distribution requires an along-strike rupture length of 72.2 km.

[22] A broader region of uplift near Quetta (Figure 7) can be explained by invoking minor slip on an uneven décollement or by invoking slip on one of several mapped listric faults near there, either before or after the 1931 earthquakes.

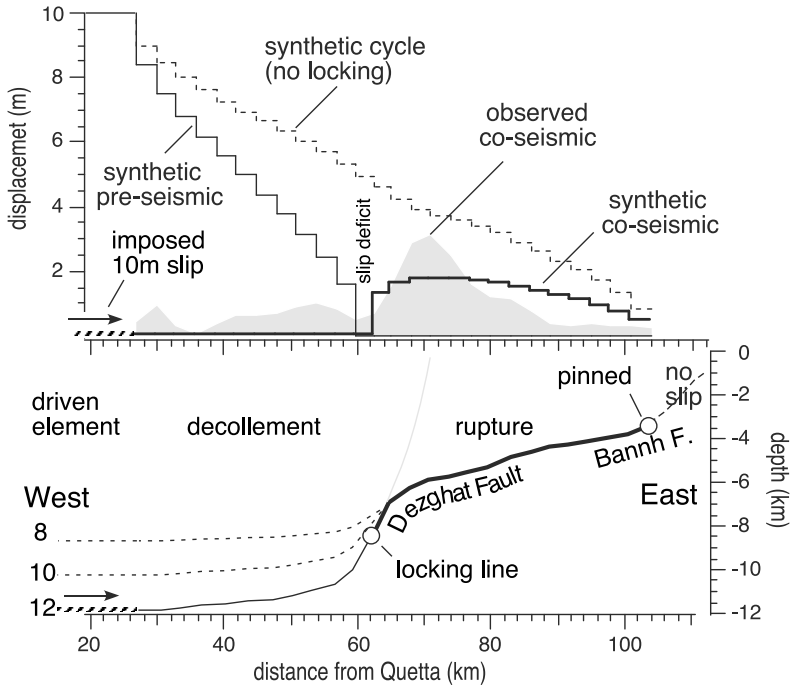

Figure 8. Geometry of the active décollement and frontal thrust (bold line with depth scale on right) and inferred slip on segments shallower than 9 km (gray envelope) compared to synthetic slip (slip scale on left). The calculated slip for the entire fault is given by the top staircase line (twenty-one 3-km-long freely slipping segments responding to an input displacement of 10 m imposed from the left (west)). The lower staircase lines are formed from two calculations: slip anticipated below a locking line at 9 km depth (synthetic preseismic slip) and the slip during rupture at shallower depths that occurs when this interseismic slip distribution drives coseismic rupture (synthetic coseismic). The difference between the two lower staircase lines and the upper staircase is the slip deficit caused by interseismic locking at 9 km depth.

We note that the fit to these minor regions of uplift in the data are nonunique since they are not constrained by well-defined subsurface geometry.

6. Discussion: The Earthquake Cycle in a Ramp-Flat-Ramp System

[23] The vertical displacement data fit in section 5 includes all deformation that occurred between 1909 and 1936. Thus the data include not only coseismic slip but possible post-seismic slip, if any occurred. We show that this is likely with a series of elastic models that assume perfectly frictionless slip below a locking line, and rupture at shallower depths (Figure 8). The models take the form of those described by *Feldl and Bilham* [2006] in which a series of contiguous, frictionless boundary elements are driven along a complex rupture surface in an uniform elastic half-space by a far-field displacement imposed at depth. The geometry of this selected far-field driving condition is not critical to the models, and similar results are obtained by imposing regional contraction on the fault system, or imposed remote thrusting. The boundary element computation calculates the amount of slip required on contiguous elements to minimize stress in their vicinity.

[24] The results from three calculations (Table 2 and Figure 8) illustrate models that emulate preseismic, coseismic slip, and finally, slip assuming no interseismic locking below the region of coseismic rupture (upper line). For the coseismic and preseismic slip calculations, the slip distribution is calculated by assuming the décollement surface is frictionless and free to slip in response to 10 m of convergence applied from the west, either for the entire fault surface (no locking) or up to a locking line at 8 or 9 km depth (preseismic). The coseismic calculation corresponds to seismic slip above the locking line, and the input to this model is the static strain field developed from the preseismic slip distribution determined from the interseismic slip calculation (Table 2).

[25] The selection of a 10-m driving displacement is arbitrary because the synthetic output scales linearly with input; however, we note that this input value results in synthetic coseismic slip that approximates the coseismic slip inferred from the leveling data. Our 10-m input condition corresponds to 2000 years of convergence at 5 mm/yr. The selection of the locking line, the transition between downdip interseismic creep and the locked seismogenic rupture zone, was investigated by running models with incrementally increased locking depths and by examining the resulting slip distribution with that inferred from the leveling data. The best fitting coseismic slip distribution occurs where interseismic

Table 3. Calculations of Partitioned Convergence[a]

Depth D (km)	Imposed S (m)	Ratio D/d	Ratio S/s
6	6	1	2
8	8.9	1.3	3
10	12	1.7	4
12	15.75	2	5.2
18	23.5	2.9	8

[a]Geometric relations between applied geodetic displacement and slip on the Dezghat/Bannh thrust fault for a range of hypothetical décollement depths (the actual depth is believed to lie in the range 18–20 km). The imposed displacement, S, is that calculated to cause the mean observed coseismic slip, s, in the Mach earthquake. D is the mean depth of the décollement, and d is the approximate starting depth of the frontal thrust above a steeper ramp connecting the two. The ratio S/s is a proxy for the increase in the recurrence interval for earthquakes on the frontal thrusts compared to the time that would be calculated from geodetic convergence rates of the entire range.

locking occurred above 8 or 9 km depth. The coseismic slip distributions resulting from locking at each of the 8- and 9-m depths are listed in Table 2.

[26] The spatial distributions of observed and synthetic coseismic slip show similarities. Peak slip in synthetic and observed data coincides in updip location but the ratio of peak slip to average slip is less in our numerical experiments than observed in the Mach earthquake. Observed slip is twice the synthetic slip at 6 km depth, and half the synthetic slip at 4.5 km depth. No simple changes in fault geometry, or freely slipping width were able to emulate the localized maximum slip at 6 km depth.

[27] The observed minimum in slip that occurs at the inferred locking line is of special interest. A significant slip deficit (3 m) occurs here as a result of preseismic and postseismic pinning at the locking line. The resulting slip deficit is analogous to the slip deficit that occurs between two contiguous strike-slip, or normal, faults that slip sequentially. *Manighetti et al.* [2005] suggests that the stresses generated by this slip deficit are released in off-fault deformation through the creation of secondary faults and folding.

[28] A paradox, however, arises in the thrust fault we are considering, for if the locking line is pinned over several earthquake cycles, the hanging wall cannot advance over the footwall. Thus although the minimum slip in the model is confirmed by the 1909–1936 leveling data, slip may occur at the locking line at times not sampled by these data. Stress conditions for slip in the region (afterslip) are most favorable for this translation shortly after the earthquake before the shallow fault "heals," yet a significant slip deficit remains 4 years after the earthquake, thus if slip occurs here it must do so over a period of many decades after each earthquake.

[29] Alternatively, if the locking line is truly locked for numerous earthquake cycles, the stored elastic energy there must eventually be released in a much larger earthquake. The significant variability in slip we see in the Mach earthquake could in fact be the result of the 1931 event being driven partly by elastic energy stored from a previous earthquake cycle. If this occurred, it would suggest that previous earthquakes terminated at a shallower locking line than that we infer for 1931. There is some evidence to suggest that the Himalaya may exhibit similar enigmatic behavior, with most décollement earthquakes associated with 3–7 m of slip and no prominent surface rupture, but with infrequent earthquakes causing surface ruptures with slip of as much as 24 m [*Feldl and Bilham*, 2006; *Bilham and Szeliga*, 2008].

[30] We discuss next the implied discrepancy between the amount of convergence (~10 m) required to drive 3 m of coseismic slip of the frontal thrust.

7. Geodetic Convergence, Slip Potential, and Renewal Time

[31] In many paleoseismic estimates of earthquake recurrence interval, the renewal time for an earthquake is estimated from the strain rate applied to a fault, a number that is derived from the present-day geodetic displacement rate measured in the region. Thus one might anticipate that a 3 mm/yr convergence rate applied to a fold and thrust belt would permit earthquakes with 3 m of slip every thousand years. Our perfectly elastic frictionless calculation indicates that the renewal of the Mach earthquake using this approach would err by a factor of 8, because only one eighth of the convergence is manifest as slip on the frontal thrust (Table 3). The remaining convergence is presumably accommodated by folding and thickening of the fold and thrust belt.

[32] The effect occurs because the ramp separating the deep décollement from the shallow frontal thrust acts as a buttress to motion. The ratio of input displacement (geodetic convergence) to frontal fault slip (measured coseismic slip) depends on the ratio of the depth of the décollement to the mean depth of the frontal thrust. As discussed in section 2 the depth of the décollement may lie at 18–20 km depth. In Figure 8 the depth of the décollement, D, is placed at 12 km depth, and the depth of the flat is ~6 km, a ratio of ~2. From a suite of numerical models in which we varied the décollement depth while maintaining the shallow geometry (Table 3) we derived the following relationship: $C = 0.00154D - 3.2$ m, where C is the (geodetic) convergence of the entire range and D is the depth of the décollement both measured in meters. The constants in the equation would be modified in systems with different shallow thrust geometries, but our basic finding would be unaltered.

[33] We find that where the décollement lies at 6 km, the renewal time is approximately doubled (Table 3) and when it lies at 10 km, the renewal time is quadrupled. Only for the case where the system is a simple planar ramp does the renewal time obey a simple 1:1 relationship between slip potential and geodetic convergence. Note that these calculations are for an infinitely long fault. By reducing the alongstrike length of the rupture the ratio of convergence to potential slip is increased yet further, as was found for the synthetic scaling law for the Himalaya [*Feldl and Bilham*, 2006]. If we use the 18–20 km depth inferred for the depth of the décollement underlying the northern Kirthar range, the Dezghat thrust "receives" only 12% of the convergence applied to the entire Kirthar range between the Chaman fault and the plains of the Indus River.

[34] How do we explain this significant discrepancy? It would appear that the ramp acts as a buttress to sedimentary layers driven from the west. Since convergence is not

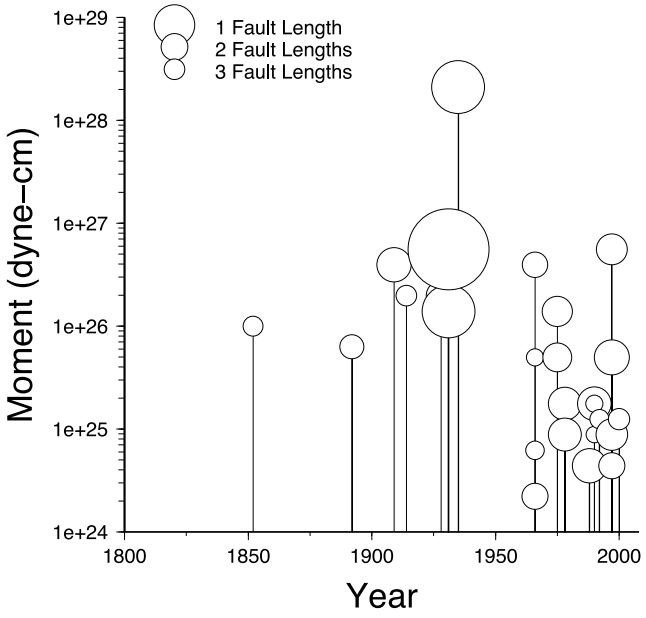

Figure 9. Space-time history of seismic moment release as a function of distance from the inferred Mach 1931 earthquake rupture zone. More than 89% of the total seismic moment release in the past 200 years (within a radius of 500 km centered on the Mach earthquake) occurred between 1931 and 1935. All known earthquakes larger than M6.5 are included.

released as slip on the shallower fault above and to the east of the ramp, it must be manifest as thickening of the sediment pile to the west. The mean topography west of the ramp is 1.5 km higher than to the east of the ramp, and the seismic section is shortened by ~15 km. East of the ramp, the frontal Dezgat/Bannh fault system has slipped by <1 km.

8. Sequential Triggering of Ruptures

[35] These three earthquakes are unusual in that most of the seismic moment release in the Baluchistan region in the last 150 years occurred within the 4 years following the first of these earthquakes (Figure 9). The clustering of these three large Baluchistan earthquakes near 30°N has a low probability of occurring by chance; hence some form of triggering appears probable. The mechanisms of stress transfer are currently speculative, especially for the first two events that occurred within 66 h of each other. No details of the Sharigh earthquake mechanism or its subsurface rupture geometry are known, and hence static stress changes cannot be computed for this event. However, the geometric relationship between the Mach and Quetta earthquakes renders a causal link substantially easier to comprehend. Rupture of the Dezgat thrust in the Mach earthquake reduced compressive east-west stresses and acted, in a sense, to unclamp the fault-normal stress on the Quetta strike-slip fault 60 km to the west. The instantaneous Coulomb failure change at Quetta is calculated to be 10 to 70 kPa depending on the nucleation depth of the Quetta earthquake, a stress change that is more than sufficient to trigger an earthquake. However, these instantaneous stress changes were apparently unimportant because the earthquake was delayed by more than 3 years. If the occurrence of the Quetta earthquake less than 4 years after the Mach earthquake is not a coincidence, we require some form of stress diffusion, or viscous creep.

[36] While poroelastic or viscoelastic processes in the body of the fold and thrust belt, or below it [*Freed*, 2005] are adequate to cause the observed delay, we consider here an alternative mechanism: viscous creep on the décollement surface. The rate of propagation of the deformation front between Mach and Quetta, had it occurred linearly, is ~18 km/yr. We note that 4 years after the earthquake we infer afterslip 10 km below the locking line to have amounted to ~1 m, with ~0.5 m of slip 20 km below the locking line. If this decay rate continued linearly downdip toward the Quetta fault, the slip on the décollement may have amounted to 10–20 cm near Quetta by 1935. The leveling data are insensitive to slip on a planar, subhorizontal surface, but the bulge in the data east of Quetta suggests that slip of some form occurred 40–50 km west from the Mach event. Slip may also have occurred prior to the Mach event in the region between Quetta and Mach, manifest as vertical changes in the 1909–1936 leveling data. We cannot exclude the possibility that aseismic or weakly seismic mobility of the structures in the fold belt prior to the earthquake sequence may have been responsible for all three events.

9. Conclusions

[37] Precise leveling data and a fault model derived from detailed geological cross sections, permit us to calculate the slip distribution on the rupture surface of the 1931 Mach earthquake. We deduce that the earthquake occurred on the 42-km-wide (E-W), 72-km-long (N-S) Dezghat/Bannh fault system west of Sibi. The fault slipped in a reverse sense up to the east with maximum slip of 3.2 m and mean slip of 1.2 m. Maximum slip coincides spatially with that predicted in elastic models driven by inferred interseismic stresses, but the maximum slip is larger than predicted compared to the mean slip of the fault. The leveling data suggest that slip also occurred downdip of the rupture (~1 m) either as afterslip or slip in other events in the interval 1909–1936.

[38] A significant (3–5 m) slip deficit remained near the interseismic locking line 4 years after the earthquake. This slip deficit may now, 67 years later, have been reduced by aseismic processes subsequent to the earthquake, or it may remain stored as elastic strain to drive future earthquakes. Two mechanisms may act to prevent the accumulation of seismic deficit over multiple earthquake cycles. The first is that slow, off-fault deformation, or pressure solution processes, act to reduce local stresses at the locking line, and the second is that infrequent larger earthquakes mine an historically stored slip deficit, accompanied by an incremental shift in the depth of the locking line. The first is testable in principle, in that we could remeasure surviving points of the leveling line to determine whether the slip deficit remains. In practice current security issues in the region render this difficult. We favor, however, the second mechanism: that

stored elastic strain from one or more previous earthquakes may account for the 3.2 m of local slip observed updip from the inferred locking line in the 1931 earthquake. The local maximum slip is easier to explain as an additional 1.5–2 m of slip inherited from strain unreleased by former earthquakes, than the alternative solution, that the slip in the earthquake should everywhere have been ~3 m in 1931 and that an ~2-m slip deficit remains on most of the fault.

[39] In considering the details of the Mach earthquake we examined in numerical experiments the elastic processes prevailing during the entire seismic cycle. We found that slip on a frontal thrust is always less than the geodetic contraction rate of a fold and thrust belt, unless the frontal thrust consists of a planar fault. In the case of a geometrically complex underlying thrust fault with variable dip, we find that partitioning of slip to the frontal thrusts is reduced in proportion to the ratio of décollement depth to shallow thrust depth where these are separated by a ramp. This significant discrepancy between the geodetic loading rate and the slip potential of frontal faults of the fold belt is presumably responsible for thickening the pile of sediments by folding and listric faulting. Partitioning in the Kirthar range, as elsewhere, results in a significantly longer renewal time for earthquakes on the frontal fault of the range, than would be derived from the geodetic convergence rate alone. Thus, although the weakly constrained 5 mm/yr GPS convergence rate between Quetta and Sibi would result in a minimum renewal time for 1.2 m (average slip) on a planar frontal thrust fault of 240 years, our study suggests that the presence of a décollement at ~18 km depth would extend the recurrence interval for Mach-type earthquakes on the Dezghat/Bannh fault system by a factor of 8, to ~2000 years.

[40] Given that more than 90% of the seismic moment release in the region occurred between 1930 and 1935 we believe that sequential triggering of the three earthquakes occurred. The 1931 Sharigh earthquake was clearly responsible for triggering the Mach earthquake 3 days later but the structural relationship between these two fault systems is obscure, and hence any attempt to explain the mechanisms involved are at present speculative. In contrast, the "broadside" relation between the Mach and Quetta rupture zones is consistent with an increase in Coulomb failure stress on the Quetta fault at the time of the Mach earthquake. The 3.5-year interval between the two earthquakes indicates, however, that static stresses changes alone were insufficient to trigger the Quetta earthquake. We hypothesize that the Mach earthquake reduced east-west stresses on the décollement/ramp system that would have facilitated accelerated creep on the basal décollement beneath the Kirthar range. Deformation between Mach and Quetta inferred from minor uplift and subsidence in the leveling data, are consistent with strain changes accompanying décollement slip, although interpretation of these data are nonunique.

[41] **Acknowledgments.** For numerous interesting discussions we are indebted to Bob Anderson, Peter Molnar, Karl Müeller, and others. We thank Andrew Meigs and an anonymous reviewer for their thorough reviews. Miriam Garcia received a UNAVCO internship and R.B. thanks Geof King and Paul Tapponier of L'institute de Physique du Globe for their hospitality during the writing of his paper. The study was funded by the National Science Foundation grants EAR003449 and EAR 0739081.

References

Ambraseys, N., and R. Bilham (2003), Earthquakes and associated deformation in northern Baluchistan, *Bull. Seismol. Soc. Am.*, *93*, 1573–1605, doi:10.1785/0120020038.

Apel, E., R. Burgmann, P. Bannerjee, and B. Nagarajan (2006), Geodetically constrained Indian plate motion and implications for plate boundary deformation, *Eos Trans. AGU*, *87*(52), Fall Meet. Suppl., Abstract T51B-1524.

Bakun, W. H., and C. M. Wentworth (1997), Estimating earthquake location and magnitude from seismic intensity data, *Bull. Seismol. Soc. Am.*, *87*, 1502–1521.

Banks, C. J., and J. Warburton (1986), 'Passive-roof' duplex geometry in the frontal structures of the Kirthar and Sulaiman mountain belts, Pakistan, *J. Struct. Geol.*, *8*, 229–237, doi:10.1016/0191-8141(86)90045-3.

Bannert, D., A. Cheema, A. Ahmed, and U. Schäffer (1992), The structural development of the western fold belt, Pakistan, *Geol. Jahrb., Reihe B*, *80*, 60, pp.

Bender, F. K., and H. A. Raza (Eds.) (1995), *Geology of Pakistan*, *Beitr. Reg. Geol. Erde*, vol. *25*, 414 pp., Gebrüder Borntraeger, Berlin.

Bernard, M., B. Shen-Tu, W. E. Holt, and D. M. Davis (2000), Kinematics of active deformation in the Sulaiman lobe and range, Pakistan, *J. Geophys. Res.*, *105*, 13,253–13,279, doi:10.1029/1999JB900405.

Bettinelli, P., J.-P. Avouac, M. Flouzat, F. Jouanne, L. Bollinger, P. Willis, and G. R. Chitrakar (2006), Plate motion of India and interseismic strain in the Nepal Himalaya from GPS and DORIS measurements, *J. Geod.*, *80*, 567–589, doi:10.1007/s00190-006-0030-3.

Beun, N., P. Border, and I. Carbonnel (1979), Premières données quantitatives relative au coulissage du décrochement de Chaman, Afghanistan du sud-est, *C. R. Seances Acad. Sci., Ser. D*, *288*, 931–934.

Bilham, R., and W. Szeliga (2008), Interaction between the Himalaya and the flexed Indian plate—Spatial fluctuations in seismic hazard in India in the past millennium?, in *2008 Seismic Engineering Conference Commemorating the 1908 Messina and Reggio Calabria earthquake*, edited by A. Santini and N. Moraci, *AIP Conf. Proc.*, *1020*(1), 224–231, doi:10.1063/1.2963839.

Day, S. M., S. H. Gonzalez, R. Anooshehpoor, and J. N. Brune (2008), Scale-model and numerical simulations of near-fault seismic directivity, *Bull. Seismol. Soc. Am.*, *98*(3), 1186–1206, doi:10.1785/0120070190.

Dziewonski, A. M., G. Ekstrom, and N. N. Maternovskaya (1999), Centroid-moment tensor solutions for October–December, 1998, *Phys. Earth Planet. Inter.*, *115*, 1–16, doi:10.1016/S0031-9201(99)00062-X.

Feldl, N., and R. Bilham (2006), Great Himalayan earthquakes and the Tibetan Plateau, *Nature*, *444*, 165–170, doi:10.1038/nature05199.

Freed, A. M. (2005), Earthquake triggering by static, dynamic, and postseismic stress transfer, *Annu. Rev. Earth Planet. Sci.*, *33*, 335–367, doi:10.1146/annurev.earth.33.092203.122505.

Garcia, M. E., W. Szeliga, and R. Bilham (2006), Modeling vertical deformation associated with the 1931 Mach earthquake, Pakistan, *Eos Trans. AGU*, *87*(52), Fall Meet. Suppl., Abstract S31A-0169.

Giardini, D., A. M. Dziewonski, and J. H. Woodhouse (1985), Centroid-moment tensor solutions for 113 large earthquakes in 1977–1980, *Phys. Earth Planet. Inter.*, *40*, 259–272, doi:10.1016/0031-9201(85)90037-8.

Haq, S. S. B., and D. M. Davis (1997), Oblique convergence and the lobate mountain belts of western Pakistan, *Geology*, *25*, 23–26, doi:10.1130/0091-7613(1997)025<0023:OCATLM>2.3.CO;2.

Herring, T. (2002), Global Kalman filter VLBI and GPS analysis program, Mass. Inst. of Technol., Cambridge.

King, R. W., and Y. Bock (2002), Documentation for the GAMIT GPS analysis software, Dep. of Earth. Atmos., and Planet. Sci., Mass. Inst. of Technol., Cambridge.

Lawrence, R. D., S. H. Khan, and T. Nakata (1992), Chaman fault, Pakistan-Afghanistan, *Ann. Tectonicae*, *6*, 196–223.

Lenox-Conyngham, G. P. (1916), *Leveling of precision in India, Addendum, Heights of bench marks*, *Sheet 39*, Surv. of India, Dehra Dun, India.

Manighetti, I., M. Campillo, C. Sammis, P. M. Mai, and G. King (2005), Evidence for self-similar, triangular slip distributions on earthquakes: Implications for earthquake and fault mechanics, *J. Geophys. Res.*, *110*, B05302, doi:10.1029/2004JB003174.

Molnar, P., and J. M. Stock (2009), Slowing of India's convergence with Eurasia since 20 Ma and its implications for Tibetan mantle dynamics, *Tectonics*, *28*, TC3001, doi:10.1029/2008TC002271.

Okada, Y. (1992), Internal deformation due to shear and tensile faults in a half-space, *Bull. Seismol. Soc. Am.*, *82*, 1018–1040.

Schelling, D. (1999), Structural geology of the Bolan block, western Pakistan, *Tech. Rep. 5-20885-99*, Energy and Geosci. Inst., Univ. of Utah, Salt Lake City.

Singh, D. D., and H. K. Gupta (1980), Source dynamics of two great earthquakes of the Indian subcontinent: The Bihar-Nepal earthquake of January 15, 1934 and the Quetta earthquake of May 30, 1935, *Bull. Seismol. Soc. Am.*, *70*(3), 757–773.

Szeliga, W., S. E. Hough, S. Martin, and R. Bilham (2009), Intensity, magnitude, location and attenuation in India for felt earthquakes since 1762, *Bull. Seismol. Soc. Am.*, in press.

West, W. D. (1934), The Baluchistan earthquakes of 25th and 27th August 1931, *Mem. Geol. Surv. India*, *67*, 1–82.

Wilson, C. A. (1938), Leveling operations, *Tech. Rep. 1937*, Surv. of India, Dehra Dun.

R. Bilham and W. Szeliga, CIRES, University of Colorado, 2200 Colorado Ave, Boulder, CO 80309-0399, USA. (szeliga@colorado.edu)

S. Lodi, Department of Civil Engineering, NED University, Karachi, 75270 Pakistan.

D. M. Kakar, Department of Geology, University of Baluchistan, Quetta, 87300, Pakistan.

D. Schelling, Structural Geology International, LLC, 474 3rd Avenue, Salt Lake City, UT 84103, USA.